



The ULR-repro3 GPS data reanalysis and its estimates of vertical land motion at tide gauges for sea level science

*Médéric Gravelle¹, Guy Wöppelmann¹, Kévin Gobron^{1,2},
Zuheir Altamimi^{3,4}, Mikaël Guichard¹, Thomas Herring⁵, Paul Rebischung^{3,4}*

¹ LIENSs, CNRS – La Rochelle University, 17000 La Rochelle, France

² Royal Observatory of Belgium, Uccle, Belgium

³ Université de Paris, Institut de physique du globe de Paris, CNRS, IGN, F-75005 Paris, France

⁴ ENSG-Géomatique, IGN, F-77455 Marne-la-Vallée, France

⁵ MIT, Cambridge, MA, USA

Correspondence to: Médéric Gravelle (mederic.gravelle@univ-lr.fr)



21 **Abstract**

22

23 A new reanalysis of GNSS data at or near tide gauges worldwide was produced by the university
24 of La Rochelle (ULR) group within the 3rd International GNSS Service (IGS) reprocessing
25 campaign (repro3). The new solution, called ULR-repro3, complies with the IGS standards
26 adopted for repro3, implementing advances in data modelling and corrections since the previous
27 reanalysis campaign, and extending the average record length by about 7 years. The results
28 presented here focus on the main products of interest for sea level science, that is, the station
29 position time series and associated velocities on the vertical component at tide gauges. These
30 products are useful to estimate accurate vertical land motion at the coast and supplement data
31 from satellite altimetry or tide gauges for an improved understanding of sea level changes and
32 their impacts along coastal areas. To provide realistic velocity uncertainty estimates, the noise
33 content in the position time series was investigated considering the impact of non-tidal
34 atmospheric loading. Overall, the ULR-repro3 position time series show reduced white noise
35 and power-law amplitudes and station velocity uncertainties compared to the previous
36 reanalysis. The products are available via SONEL (https://doi.org/10.26166/sonel_ulr7a;
37 Gravelle et al., 2022).



38 1 Introduction

39

40 Vertical land motion plays a crucial role in understanding sea level changes and its spatial
 41 variability (Wöppelmann & Marcos, 2016; Frederikse *et al.*, 2020; Hamlington *et al.*, 2020; for
 42 recent reviews and references therein). This is especially true along the coasts, where its
 43 monitoring is often an essential requirement to assess the extent of the environmental and socio-
 44 economic threats posed by changing sea levels in a warming climate at regional or local scales
 45 (Magnan *et al.*, 2020). Changes in sea level can be measured relative to the land by tide gauges,
 46 or relative to the Earth's center of mass by satellite altimeters (e.g., Marcos *et al.*, 2019). In
 47 both relative (tide gauge) and geocentric (satellite) measuring systems, accurate estimates of
 48 vertical land motion are essential, either to disentangle the solid Earth contribution from other
 49 factors in tide gauge records (Woodworth *et al.*, 2019), or to supplement satellite altimetry data
 50 to assess relative sea level change for coastal studies and planning (Poitevin *et al.*, 2019).

51

52 In the last decades, significant efforts have been undertaken to produce accurate estimates of
 53 vertical land motion at tide gauges using Global Navigation Satellite System (GNSS) data (e.g.,
 54 Sanli and Blewitt, 2001; Wöppelmann *et al.*, 2007; Hammond *et al.*, 2021). Wöppelmann *et al.*
 55 (2007) showed the importance of applying a homogeneous GNSS data reanalysis strategy
 56 across the entire data span; that is, using the same modelling, corrections and parameterization,
 57 to address the demand of accurate position time series and velocities for sea level studies. This
 58 conclusion was reached independently by Steigenberger *et al.* (2006) within the International
 59 GNSS Service (IGS; Johnston *et al.*, 2017). Since then, the IGS has conducted several data
 60 reanalysis campaigns, stimulated by progress in modelling and corrections, lengthening of
 61 measurement records and updates of the International Terrestrial Reference Frame (ITRF)
 62 realizations (Rebischung *et al.*, 2016).

63

64 In 2019, the IGS launched a third reprocessing campaign, designated as 'repro3', involving the
 65 international GNSS community (Rebischung, 2021). The University of La Rochelle (ULR)
 66 group contributed to this effort with a solution (ULR-repro3), that specifically includes a large
 67 selection of reliable GNSS stations near tide gauges. This paper describes the latest ULR
 68 solution in a series, complying with the modelling and corrections adopted for 'repro3'
 69 (Rebischung, 2021; <http://acc.igs.org/repro3/repro3.html>), which succeeds previous releases
 70 (Wöppelmann *et al.*, 2009; Santamaria-Gomez *et al.*, 2017). It specifically highlights the time
 71 series of station positions and their vertical velocities, which are the main products of interest



72 for the sea level community. A crucial piece of information for the practical use of these
 73 products is their uncertainties, which must account for the presence of time-correlated
 74 stochastic variations (or noise) in the position time series (Williams *et al.*, 2004). Consequently,
 75 this paper also presents the statistical modelling strategies employed to derive realistic
 76 uncertainty estimates. These results are presented together with a comparison with respect to
 77 the previous ULR solution to appraise the progress accomplished over the past seven years.

78

79 **2 The ULR-repro3 products**

80 **2.1 Input data**

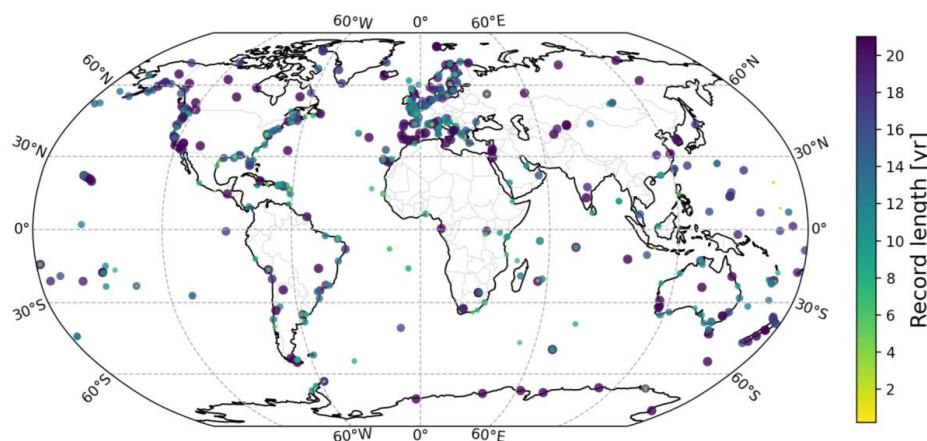
81 Although the term GNSS is employed throughout the manuscript, the ULR-repro3 reanalysis
 82 considered Global Positioning System (GPS) observations only. The GNSS measurements were
 83 retrieved from the SONEL archive (www.sonel.org) in the form of station-specific daily files
 84 in the international standard RINEX format. These contain dual-frequency carrier phase and
 85 pseudo-range measurements with a typical sampling of 30s. SONEL holdings include data from
 86 over 1,200 stations around the world, amounting to over 6,300,000 daily files. A station
 87 selection was applied with the criteria of targeting time series with over three years of
 88 continuous GNSS measurements and 70% completeness, located at or near a tide gauge. The
 89 term “continuous” denotes that no offset discontinuity in the station position was anticipated
 90 from the metadata available, that is, from the station operation logfiles, which should report
 91 changes in instrumentation, or from the co-seismic displacements predicted using the
 92 earthquakes database and modelling described by Métivier *et al.* (2014), updated to 2020. Some
 93 exceptions to these selection criteria concerned the French GNSS stations at tide gauges, as part
 94 of the ULR commitment for France to the global sea level observing (GLOSS) programme of
 95 the Intergovernmental Oceanographic Commission (IOC, 2012).

96

97 The spatial distribution of the GNSS stations considered in ULR-repro3 is shown in Figure 1
 98 with symbols colored according to the record length, ranging from 3 months to 21 years. The
 99 last year processed is 2020, instead of 2013 for the previous ULR reanalysis (Santamaria-
 100 Gomez *et al.*, 2017), reaching an overall extension of seven years with a median station record
 101 length of 13.1 years. The station network shows a global distribution (Figure 1) with stations
 102 that are obviously far from coastlines: they were added from the IGS repro3 station priority list
 103 as reference frame stations to ensure an optimal alignment to the International Terrestrial



104 Reference Frame (ITRF) and estimation of the satellite orbits. The ULR-repro3 station network
 105 ultimately consists of 601 GNSS stations (Figure 1).



106
 107 **Figure 1:** Spatial distribution of the 601 GNSS stations in ULR-repro3 and record length (colorbar),
 108 whose median is 13.1 years, spanning the 2000.0-2021.0 period.

110 2.2 GNSS processing

111 Estimating accurate vertical land motion from GNSS measurements involves several essential
 112 steps, such as computing daily station positions from GNSS measurements or deriving trends
 113 from the position time series. In the first step, many corrections are applied, and other
 114 parameters such as satellite orbits or atmospheric delays are adjusted along with the station
 115 positions. It requires advanced modelling and corrections (details below) and is usually best
 116 performed in a free-network approach or loosely constrained strategy (Heflin *et al.*, 1992;
 117 Altamimi *et al.*, 2002), whose major output is a global set of daily station positions expressed
 118 in an undetermined terrestrial frame. The next step is to align these global solutions of daily
 119 station positions to a stable and well-defined terrestrial frame such as the ITRF2014 (Altamimi
 120 *et al.*, 2017). The last step involves modelling the kinematics described by the position time
 121 series, to obtain the quantity of interest (trends, periodic oscillations, step discontinuities, etc.).
 122 Each step involves analyst choices that can affect the estimated quantity of interest, and
 123 subsequently the geophysical interpretation. The details below can thus be crucial to understand
 124 the results and their uncertainties.

125



126 2.2.1 Modelling & Corrections

127 The ULR-repro3 processing considered the advances that occurred over the past seven years,
 128 since the second IGS reanalysis campaign (Reischung *et al.*, 2016). It complies with the
 129 highest international standards, which were adopted by the IGS for the third reprocessing
 130 campaign (<http://acc.igs.org/repro3/repro3.html>). The new modelling and corrections were
 131 implemented in the GAMIT/GLOBK software packages (Herring *et al.*, 2015; 2018) used here,
 132 in particular the International Earth Rotation and Reference Systems Service (IERS) linear pole
 133 model adopted in 2018 and the high-frequency (subdaily) Earth Orientation Parameters (EOP)
 134 tide model from Desai and Sibois (2016). Table 1 provides a summary of the main modelling
 135 features and corrections applied in the ULR-repro3 reanalysis.

136
 137 **Table 1:** Main features of the GNSS data analysis strategy adopted for ULR-repro3 following
 138 the IGS recommendations (<http://acc.igs.org/repro3/repro3.html>).

ULR-repro3 modelling and corrections	
Observations	double-differenced phase observations (GPS only, L1 & L2)
Sessions and sampling	24-hr sessions; 2 min. sampling (30s in the data cleaning)
Elevation cut-off angle	10 degrees
Antenna phase center	igsR3_2135.atx (IGS Mail by A. Villiger, Dec. 2020)
Ionosphere refraction	ionosphere-free linear combination (1st order effect); 2nd and 3rd order corrections using IGRF13 (Alken <i>et al.</i> , 2021) and IGS IONEX files.
Troposphere refraction	A priori zenith delays from Saastamoinen model, mapped with VMF1 functions (Böhm <i>et al.</i> , 2006); zenith wet delays estimated at 1-hr intervals and gradients in north-south and east-west directions at 24-hr intervals.
Gravity field model	EGM2008 up to degree and order 12 (Pavlis <i>et al.</i> , 2012)
Solid Earth tides	IERS conventions (Petit & Luzum, 2010)
Ocean tide model	FES2014b (Lyard <i>et al.</i> , 2021)
Mean pole	linear mean pole as adopted by IERS in 2018
Subdaily EOP model	Desai & Sibois (2016)
Ocean tide loading	Provided by the EOST loading service (J.P. Boy; http://loading.u-strasbg.fr) using the ocean tide model FES2014b (Lyard <i>et al.</i> , 2021)

139
 140 The remaining aspects of the ULR-repro3 data analysis strategy align with the approach used
 141 in Santamaria-Gomez *et al.* (2017), so the following only briefly outlines them to understand
 142 the analyst choices for geophysical application and interpretation. For each network of stations,
 143 double-differenced GPS phase observations were processed in the ionosphere-free L1/L2 linear
 144 combination. To minimize the impact of mismodeled low-elevation tropospheric delays,



145 satellite observations below 10 degrees were not considered. This cut-off angle aims to mitigate
 146 the limitation due to ground antennas without absolute calibration (13% of the antennas in the
 147 ULR-repro3 network), converted from relative to absolute considering only elevation-
 148 dependent phase center variation (PCV) down to 10 degrees. For the other (calibrated) GNSS
 149 antennas, phase center offsets with azimuth-dependent and elevation-dependent absolute PCV
 150 corrections were applied (igsR3_2135.atx; IGS Mail by A. Villiger, 2020). Satellite-specific
 151 antenna phase center offsets and block-specific nadir angle-dependent absolute PCV were
 152 applied for the transmitting antennas.

153

154 The first-order ionospheric delays were removed using the ionosphere-free linear combination
 155 observations, whereas the second and third orders were corrected using the International
 156 Geomagnetic Reference Field model (Alken *et al.*, 2021) and total electron content maps from
 157 the IGS IONEX files. For the tropospheric delays, a priori hydrostatic zenith delays at the
 158 ellipsoidal surface were obtained for each station from the VMF1 grids (Böhm *et al.*, 2006).
 159 They were then reduced to the station heights using the GPT2 model (Lagler *et al.*, 2013). The
 160 residual zenith tropospheric delays were adjusted at 1-hr intervals (i.e., 25 parameters per day)
 161 for every station using a piecewise linear model, assuming the unmodeled wet component
 162 dominates. Both the hydrostatic and wet zenith tropospheric delays were mapped to the
 163 observation elevations using the VMF1 functions. The azimuthal asymmetry in the tropospheric
 164 delay was accounted for by estimating a linear change in gradients (north-south and east-west)
 165 over each day and station using the mapping function from Chen and Herring (1997).

166

167 The phase observations were weighted by elevation angle in the first iteration, and then by
 168 elevation angle and station-dependent scatter of the phase residuals obtained from the first
 169 iteration. The double-differenced phase ambiguities were adjusted to real values except when
 170 they could be confidently fixed to integer values (more than 85% fixed). Within the same
 171 inversion, GNSS satellite orbital parameters were adjusted using 24-hr arcs, IGS orbits as a
 172 priori values and loose constraints consistent with the station position constraints (free-network
 173 approach). Non-gravitational constant and once-per-revolution accelerations on the satellites
 174 were adjusted too, using the ECOMC model (combination of the ECOM1 and ECOM2 models
 175 (Springer *et al.*, 1999; Arnold *et al.*, 2015) with specific parameters constrained in post-
 176 processing). Nominal satellite attitude corrections were applied, except during eclipse periods
 177 where yaw rates were modelled (Kouba, 2009). Phase rotations due to changes in the satellite
 178 antenna orientation away from the Earth-pointing direction were also applied (Wu *et al.*, 1993).



179 Regarding the Earth orientation parameters (pole position, rate and length of day), these were
 180 estimated daily with a priori values from the IERS Bulletin A. Modeled diurnal and semi-
 181 diurnal terms were added to the a priori pole and UT1 values following the IERS Conventions
 182 (Petit and Luzum, 2010).

183

184 Note that neither loading displacements due to atmospheric tides nor non-tidal (atmospheric,
 185 oceanic, hydrology) loading displacements were corrected during the first step, which aimed at
 186 estimating daily station positions from the GNSS measurements. By contrast, the displacements
 187 of the crust due to solid-Earth and pole tides (solid Earth and ocean) were corrected following
 188 the IERS Conventions (Petit and Luzum, 2010). Crustal motion due to the ocean tide loading
 189 was corrected too, using the tidal constituents computed by EOST loading service at each
 190 station from the FES2014b model (Lyard *et al.*, 2021).

191

192 ***2.2.2. Offset detection & terrestrial frame alignment***

193 Figure 2 shows the number of stations selected for ULR-repro3 with GNSS observations
 194 available each day over the time period considered (2000.0-2021.0), ranging from 110+ to
 195 nearly 500 stations. For computational efficiency, the stations were split into several regional
 196 subnetworks, each having between 29 and 70 stations processed independently. An additional
 197 subnetwork of globally distributed stations was considered to allow the daily combination of
 198 the regional subnetwork results in a unique daily global solution. This global subnetwork was
 199 made up of IGS reference frame stations, each of which also appeared in one – and only one –
 200 of the regional subnetworks. In turn, one regional subnetwork included one IGS reference frame
 201 station at least, but could include more depending on the total number of subnetworks.
 202 Moreover, to strengthen the physical link between regional subnetworks, two stations from
 203 adjacent regional subnetworks were also included, that is, one station from one nearby
 204 subnetwork and another from another nearby subnetwork, exclusive of the stations in the global
 205 subnetwork. This network strategy has changed compared to past ULR reanalyses, benefitting
 206 from the experience of the Massachusetts Institute of Technology (MIT) IGS analysis center.

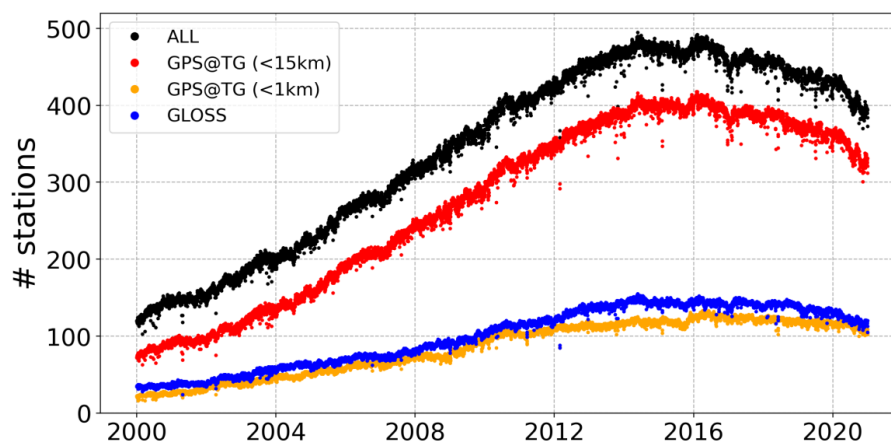


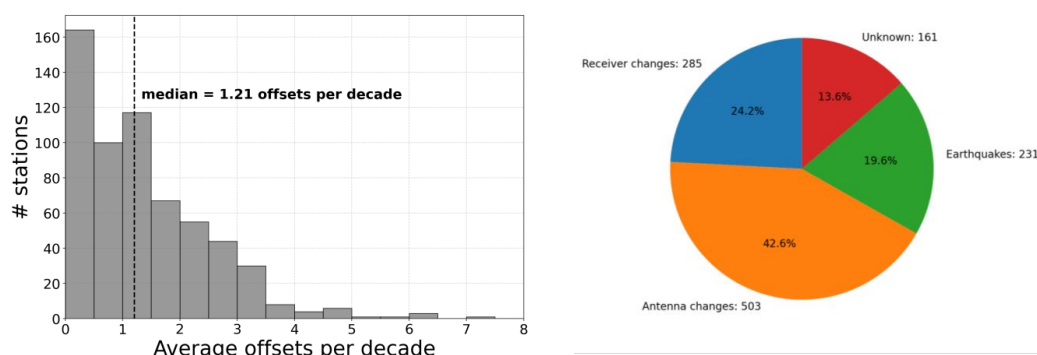
Figure 2: Evolution of station availability in ULR-repro3 (all in black), within 15 km and 1 km distance from a tide gauge (red and orange, respectively), and GLOSS tide gauge site (blue)

The loosely-constrained station positions and tropospheric delays for the common stations and the satellite orbital and Earth rotation parameters estimated from the subnetwork data analyses were combined using GLOBK (Herring et al., 2021) to obtain the daily global solutions, which include all stations available each day with their positions expressed in a common but yet undetermined terrestrial frame. These daily global solutions were then stacked into a long-term solution using the CATREF software package (Altamimi *et al.*, 2018) with a time-dependent functional model that included translation, rotation and scale transformation parameters between daily and long-term frames, estimated simultaneously with the mean station positions (at the reference epoch 2010.5), annual and semi-annual signals and velocities. The scale parameters, that represent the mean height changes of all the sites, are available upon request, especially for users interested in global sea level rise.

Note that position offset discontinuities (mostly due to equipment changes and earthquakes), as well as station velocity changes and post-seismic displacements, were added to the above modelling, where appropriate. Since experimented analysts still tend to perform better than automatic methods (Gazeaux *et al.*, 2013), the position offsets were identified and adopted by expert eyeball using all positioning components (i.e., including north and east components). To facilitate this task, the equipment changes reported in the GNSS station logs were considered, as well as the co-seismic displacements larger than 2 mm predicted with the earthquakes



230 database and modelling by Métivier *et al.* (2014). When a position discontinuity was detected
 231 in a time series, the station position was estimated separately before and after the discontinuity
 232 together with the offset amplitude. The velocities before and after each position discontinuity
 233 were tightly constrained (0.01 mm/yr), unless a velocity discontinuity was suspected. In the
 234 latter case (less than 2% of the GNSS stations considered in ULR-repro3), no constraint was
 235 applied and different velocities were estimated for each period of data around the discontinuity.



236 **Figure 3:** Average station position offsets per decade (histogram) and offsets origin (piechart)

237

238 The above procedure also included manual editing to identify (and remove) outliers as well as
 239 additional non-documented position offset discontinuities. It was iterated until convergence
 240 (expert eyeball). Overall 1.2 offset discontinuities were detected per decade, mostly caused by
 241 equipment changes (66.8%) and earthquakes (19.6%), whereas the remaining 13.6% were
 242 flagged as unknown (Figure 3) due to the lack of available metadata.

243

244 The long-term terrestrial frame, in which the estimated velocities are ultimately expressed, was
 245 finally aligned to the ITRF2014 (Altamimi *et al.*, 2017) by applying minimal constraints to all
 246 the transformation parameters (translation, rotation, scale, and their rates) with respect to the
 247 positions and velocities of a stable subset of about 35 well-distributed reference frame stations.
 248 This step resulted in daily position time series expressed in the ITRF2014 frame for all (601)
 249 stations considered in ULR-repro3. From this set of position time series, only stations having
 250 more than three years between two consecutive position discontinuities and with data gaps not
 251 exceeding 30% were retained for the next step as input.

252



253 2.2.3. Stochastic modelling and time-correlated noise

254 The last step was the estimation of the parameters of interest (primarily here station velocities)
 255 and their uncertainties, where both a functional and a stochastic model were adjusted to each of
 256 the position time series from the previous step on a station by station basis. In this step, an
 257 additional and independent time series editing was considered to eliminate possibly remaining
 258 unreliable estimates from the previous step. The position estimates were compared to a running
 259 monthly median. Any epoch with a position showing a difference from the median exceeding
 260 five times the median absolute deviation in at least one component was discarded.

261

262 The stochastic model considered a linear combination of white noise and power law process
 263 (WN+PL), whose parameters (the stochastic process amplitudes and the spectral index of the
 264 power-law process) were estimated using the Restricted Maximum Likelihood Estimation
 265 method (Patterson & Thompson, 1971; Koch, 1986; Gobron *et al.*, in press). To obtain realistic
 266 stochastic parameter estimates, non-tidal atmospheric loading (NTAL) displacements were also
 267 subtracted from the position time series prior to this adjustment, following the recommendation
 268 of Gobron *et al.* (2021). These NTAL displacements were obtained from the Earth System
 269 Modelling team of the German research center for geosciences in Potsdam (Dill and Döbrowsky,
 270 2013).

271

272 The functional model included an intercept, a linear trend (velocity), the position offsets
 273 identified in the previous step, three seasonal terms (annual, semiannual, and terannual),
 274 periodic terms at the first eight harmonics of the GPS draconitic year (351.4 days; Ray *et al.*,
 275 2008), and three fortnightly terms with periods of 13.62, 14.19 and 14.76 days (Penna and
 276 Stewart, 2003; Amiri-Simkooei, 2013). The parameters of this functional model, and their
 277 uncertainties, were estimated using the weighted least squares estimator with the inverse of the
 278 estimated WN+PL model covariance matrix as weight matrix. During the observation time
 279 span, some stations (44) recorded significant co-seismic offsets and transient post-seismic
 280 signals, in which case the modeling was further extended to include velocity changes, and
 281 logarithmic or exponential decay functions according to the observed time evolution.

282



2.3 Estimates of vertical land motion

2.3.1 Position time series & Vertical velocities

The GNSS products of primary interest for sea level studies are the station position time series and velocity estimates on the vertical component, as underlined in the founding charter of the IGS working group “GNSS Tide Gauge Benchmark Monitoring” (Schöne *et al.*, 2009) and later on in the implementation plan of the GLOSS programme (IOC, 2012). In the following, we focus on the vertical positioning component. However, the horizontal components are made available too, and can be useful for other geophysical applications. Figure 4 shows the ULR-repro3 vertical velocity field, and the corresponding uncertainties. This GNSS velocity field ultimately consists of 546 stations, among which 457 are within 15 km from a tide gauge. This number decreases to 135 for stations less than 1 km from a tide gauge. Note that the stations inland are IGS reference frame stations (section 2.1).

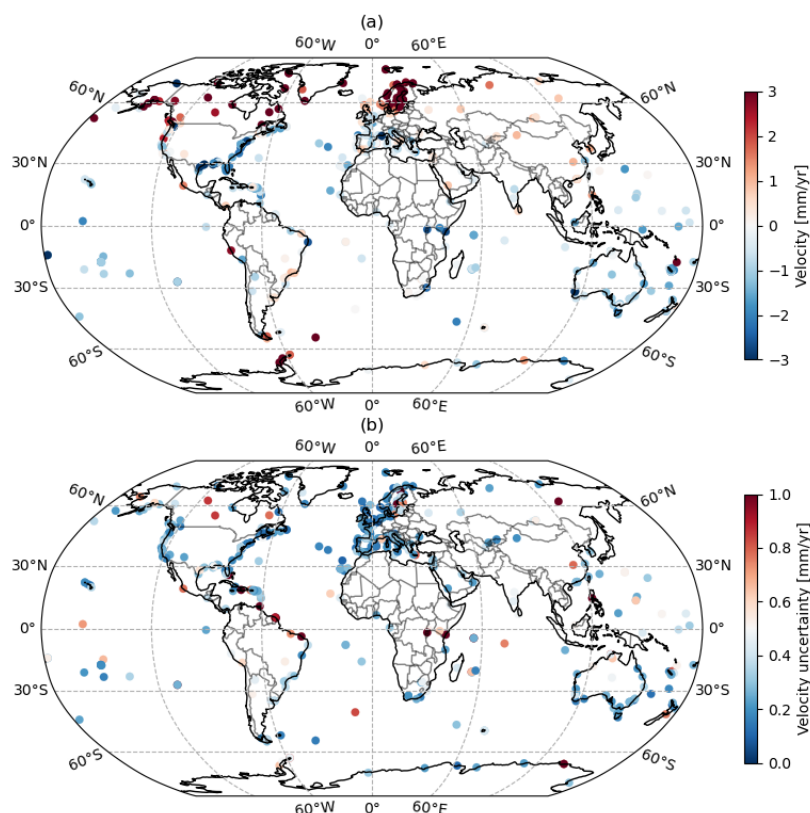


Figure 4: Vertical velocities (a), and associated uncertainties (b), estimated for the stations with at least 3 years of continuous measurement (see text).



Overall, the geographical patterns observed in Figure 4.a are consistent with known geophysical processes such as uplift in the northern latitudes of Europe and America due to Glacial Isostatic Adjustment (GIA), or subsidence along the northern coastlines of the Gulf of Mexico primarily driven by ground water depletion and sediment compaction, also observed in previous and independent GPS analysis results (e.g., Blewitt *et al.*, 2018; Hammond *et al.*, 2021). Stations with velocity discontinuities are not plotted in Figure 4.

2.3.2 Data availability

The ULR-repro3 products are available from the online Digital Object Identifier (DOI) landing page (https://doi.org/10.26166/sonel_ulr7a; Gravelle *et al.*, 2022). That is, the station position time series together with the estimated velocities for all positioning components (north, east, and up). These products are hosted at the SONEL scientific service, which serves as data assembly center dedicated to GNSS data at tide gauges (Wöppelmann *et al.*, 2021) for the international GLOSS programme (IOC, 2012). As a UNESCO-related programme, the service complies with the UNESCO open access data policy (i.e., the data sets are available free of charge without any barriers) and strives towards providing the highest international standards, in particular in terms of long-term availability and permanent access. Note that the ULR-repro3 reanalysis yielded other parameter estimates, which can be of interest to other geophysical applications (e.g., station position offsets related to earthquakes and seasonal signals). These are also made available via SONEL.

3 Products quality

3.1 Average time correlation properties

Previous studies have documented the presence of both power-law noise and white noise in GNSS station position time series (e.g., Williams *et al.*, 2004; Santamaria-Gomez *et al.*, 2011; Gobron *et al.*, 2021; Santamaria-Gomez & Ray, 2021). Such time-correlated properties are also observed in Figure 5 for ULR-repro3, where Lomb-Scargle periodograms of all detrended station positions time series were averaged. In logarithmic scales, the power-law process induces the negative trend at low frequencies (that is, a spectral power $\propto 1/f^\alpha$), whereas the white noise causes the flattening at high frequencies. This flattening is especially visible above 22.8 cpy, where the power of the white noise exceeds that of the power-law process.

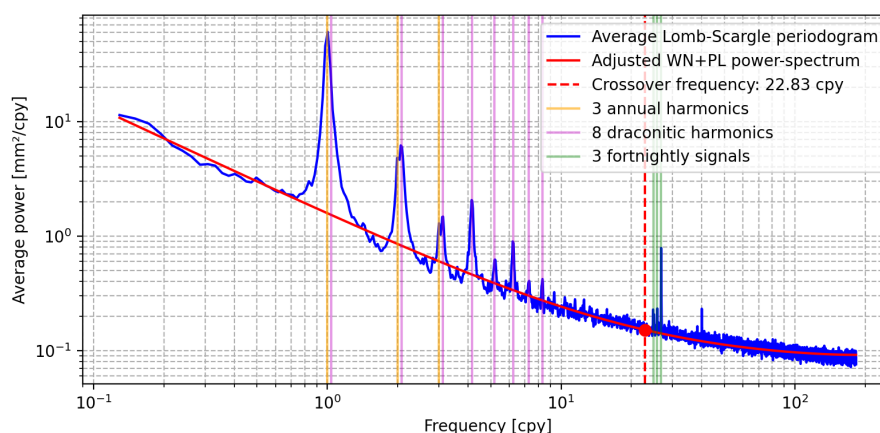
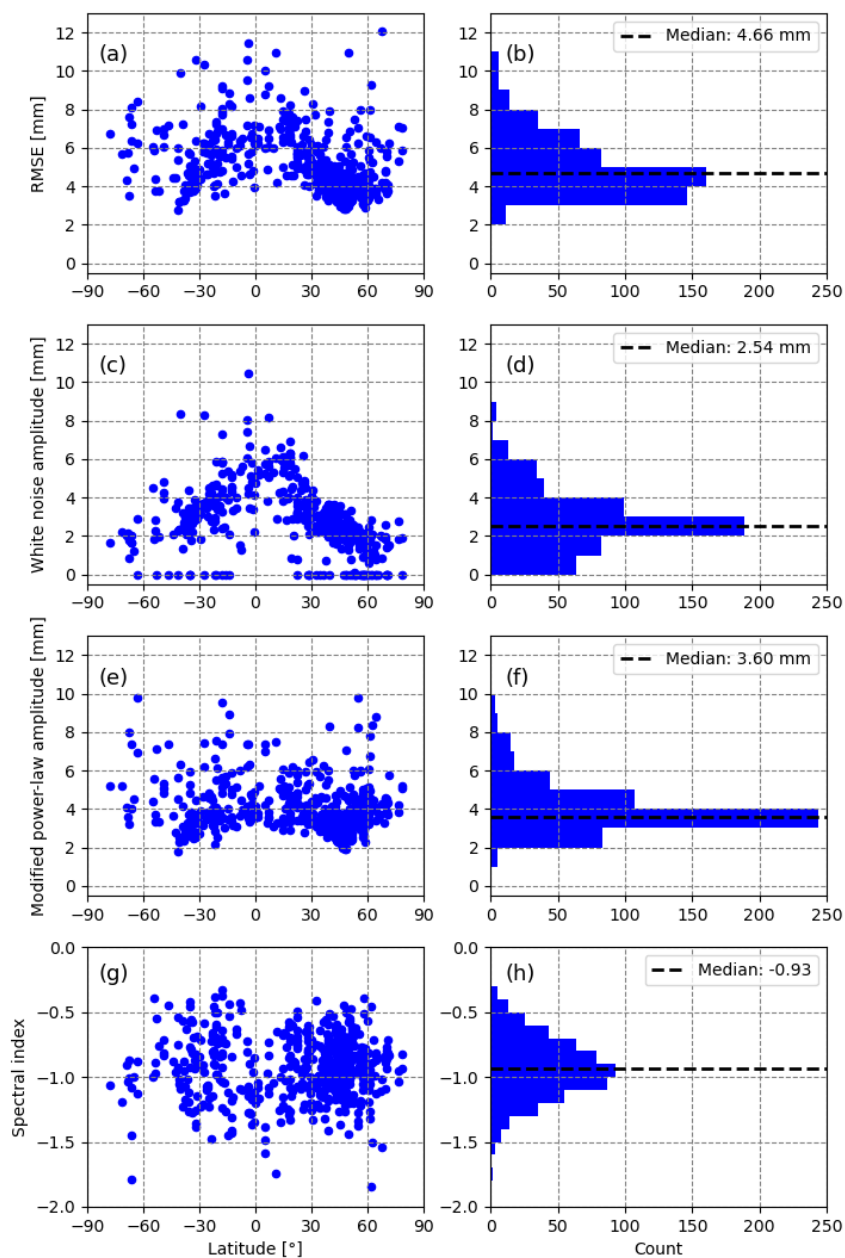


Figure 5: Average Lomb-Scargle periodogram for the ULR-repro3 detrended vertical position time series corrected for NTAL displacements (frequency unit is cycles per year or cpy).

3.2 Stochastic properties of position time series

As the periodogram does not provide information about the properties of individual stations, the parameters, namely, the stochastic process amplitudes and the spectral index, the WN+PL stochastic models adjusted to the individual vertical position time series are presented in Figure 6.

The median value of the spectral indices is -0.93, that is, close to -1.00, which confirms the prevalence of a flicker-like noise in the low frequency band. The spectral indices show no clear latitudinal dependency (Figure 6.g-h). Since power-law amplitudes depend on the spectral index values, they were transformed into a modified empirical standard deviation (Gobron *et al.*, 2021), expressed in mm, enabling a more rigorous comparison between noise amplitudes and Root Mean Squared Errors (RMSE) values. No latitudinal dependency is revealed in Figure 6.e. By contrast, the white noise amplitudes show largest values within the tropical band (Figure 6.c), and lower values at high latitude, but mostly non-zero thanks to the NTAL corrections (Gobron *et al.*, 2021). Logically, this pattern also appears in the RMSE (Figure 6.a), as it quantifies the combined influence of the white noise and power-law processes.



351

352 **Figure 6:** Vertical position time series RMSE (a) and (b), white noise amplitudes (c) and (d); modified
 353 power-law amplitudes (e) and (f); and spectral indices (g) and (h). See text for details.

354



3.3 Vertical velocity uncertainties

An important consequence of temporally correlated noise in time series of GNSS positions is its impact on the uncertainties of GNSS-derived velocities, which can be largely underestimated, up to a factor of ten (Williams *et al.*, 2004), if the temporal correlations are ignored. Figure 7 shows the distribution of the vertical velocity uncertainties obtained for the ULR-repro3 stations considering the stochastic properties estimated above. Their median value is 0.27 mm/yr with 83% of the stations displaying a vertical velocity uncertainty below 0.5 mm/yr. The coloring in Figure 7.a indicates that the largest velocity uncertainties typically correspond to the stations with the shortest records.

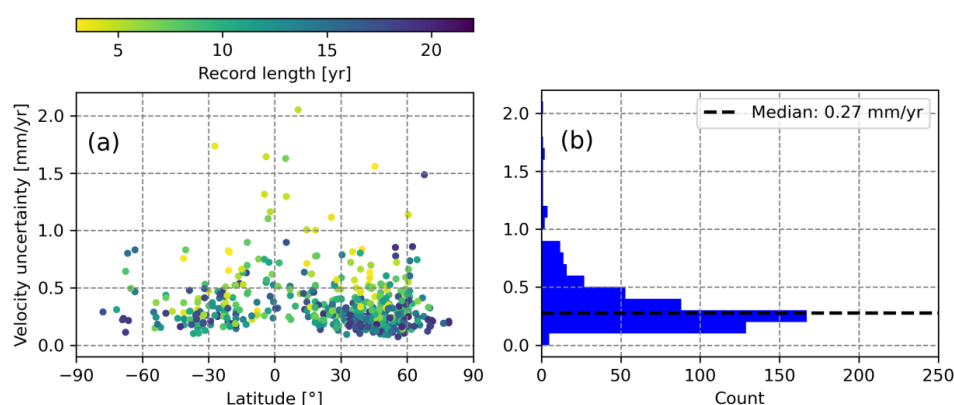


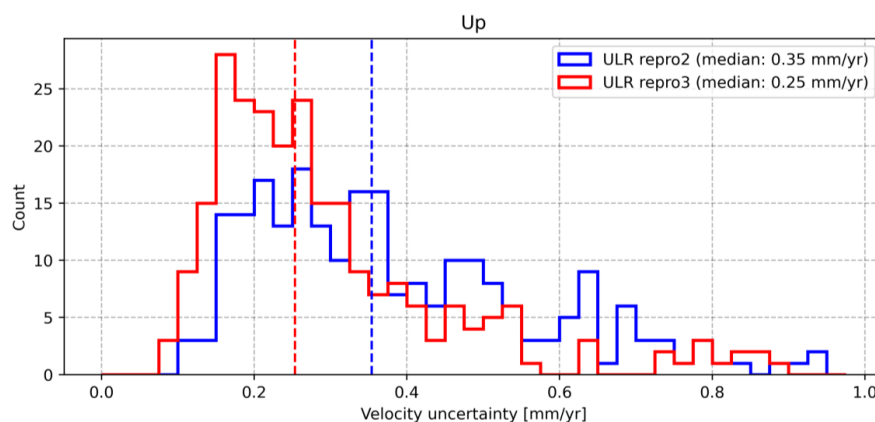
Figure 7: Vertical velocity uncertainties as a function of the geographical latitude with color corresponding to the record length (a) and histogram (b).

3.4 Highlights wrt previous ULR reanalysis

To appraise the progress accomplished with the ULR-repro3 reanalysis, the position time series from the previous reanalysis (Santamaria-Gomez *et al.*, 2017) were retrieved at SONEL, and the same processing (last step in section 2) was applied for a rigorous comparison (same non-tidal atmospheric loading corrections, and same functional and stochastic models). This comparison involved the 251 common stations. Figure 8 indicates a substantial reduction of 28% in the median vertical velocity uncertainties, from 0.35 mm/yr down to 0.25 mm/yr (ULR-repro3), which is below the uncertainty threshold reported by Griffiths and Ray (2016) using simulations to investigate the effect of position offsets and record lengthening. However, it is worth noting that the community interested in monitoring vertical land motion at tide gauges tend to limit changes in GNSS equipment to the strict unavoidable (failure, destruction, etc.) as recommended by the IGS-related working group (Schöne *et al.*, 2009). As a result, the average



380 return period of offsets is about four years longer here (Figure 3) than observed for the entire
 381 set of stations contributing to the IGS repro3 campaign (Rebischung *et al.*, 2021), hence partly
 382 explaining the improved velocity uncertainties observed with ULR-repro3 reanalysis.
 383



384
 385 **Figure 8:** Vertical velocity uncertainties for ULR-repro3 wrt the previous ULR solution based on the
 386 251 common stations. The vertical dashed lines correspond to the medians.

387
 388 The marked improvement in the quality of ULR-repro3 products can also be appraised from
 389 the RMSE position residuals (median value of 5.3 mm down to 4.9 mm now) and the amplitude
 390 of white noise (from 3.4 mm to 2.8 mm), whereas the power-law amplitude and spectral index
 391 remained equivalent (3.8 mm and -0.93, respectively).
 392

393 4 Concluding remarks

394 This paper has presented the latest GNSS data reanalysis carried out by the ULR group within
 395 the international IGS framework, yielding time series of position estimates to measure the
 396 vertical land motion nearby tide gauges. It includes an increased number of GNSS stations with
 397 an extended time span. Along with the velocity estimates, their uncertainties were obtained by
 398 modelling the temporally correlated noise processes inherent in the data, after correcting the
 399 position time series for non-tidal atmospheric loading displacements, as recommended by
 400 Gobron *et al.* (2021). Overall, the comparisons indicate that ULR-repro3 represents a marked
 401 improvement in its products quality over the previous reanalysis, with a notable reduction in
 402 median velocity uncertainty by 28% (Figure 8).



An interesting perspective will be to examine the differences with global reanalyses obtained by other groups complying with the latest IGS standards, but using different analyst choices at any of the major GNSS processing steps described in section 2 (e.g., Blewitt *et al.*, 2016; Männel *et al.*, 2022). A related perspective will be to address the issue of which reanalysis is best for the non-expert sea level user, if any (Ballu *et al.*, 2019). In this respect, the Commission on mean sea level and tides from the International Association for the Physical Sciences of the Oceans (IAPSO) could provide a stimulating framework to gather experts and users worldwide, and reflect on the issue posed by multiple high-quality GNSS reanalyses, as IAPSO did nearly thirty years ago when the issue of geodetic fixing of tide gauge benchmarks was considered with the advances of space geodesy (Carter *et al.*, 1994).

Acknowledgments

This study was financially supported by the CNRS/INSU research agency via the SONEL & RENAG observation systems. Our study benefited tremendously from agencies making their data available to IGS and SONEL. The authors would like to acknowledge the crucial role played by the high-performance computing center of La Rochelle University, especially with Mozart & Thor supercomputers. Part of this research were made possible by support from NASA grant 80NSSC18K0457 and NSF grant NSF-IF-1843686. This is IPGP contribution number XXXX. We are grateful to Laurent Métivier for providing the modeled earthquake displacements and Jean-Paul Boy for the ocean tidal loading corrections.

Author contributions

The project was defined by MGr and GW as a contribution to the third reprocessing (‘repro3’) campaign of the International GNSS Service (IGS). MGr processed the GPS data with support from TH (GAMIT/GLOBK software packages, network design, and strategy for subnetwork design and orbit adjustment), ZA (CATREF software and reference frame alignment), PR (product quality assessment within ‘repro3’), and MGu (strategic use of the high-performance computing center). KG prepared the NTAL corrections, assessed the stochastic properties of the time series and produced the final velocity field. All authors contributed to the analysis and discussion of the results. The first manuscript draft was written by GW. All authors contributed to the subsequent versions, and approved the final manuscript.

Competing interests

The contact author has declared that none of the authors has any competing interests.



437 References

- 438 1. Alken, P., Thébaud, E., Beggan, C.D., et al.: International Geomagnetic Reference
 439 Field: the thirteenth generation. *Earth Planets Space*, 73, Art. 49, doi:10.1186/s40623-
 440 020-01288-x, 2021.
- 441 2. Altamimi, Z., Boucher, C., and Sillard, P.: New trends for the realization of the
 442 International Terrestrial Reference System, *Adv. Sp. Res.*, 30, 175-184, 2002.
- 443 3. Altamimi, Z., Métivier, L., Rebischung, P., Rouby, H., and Collilieux, X.: ITRF2014
 444 plate motion model, *Geophys. J. Int.*, 209, 1906-1912, 2017.
- 445 4. Altamimi, Z., Boucher, C., Sillard, P., Collilieux, X., and Rebischung, P.: CATREF
 446 software (Combination and Analysis of Terrestrial Reference Frames), Manual,
 447 version of April 19th, 2018.
- 448 5. Amiri-Simkooei, A.R.: On the nature of GPS draconitic year periodic pattern in
 449 multivariate position time series, *J. Geophys. Res.: Solid Earth*, 118, 2500-2511,
 450 doi:10.1002/jgrb.50199, 2013.
- 451 6. Arnold, D., Meindl, M., Beutler, G., Dach, R., Schaer, S., Lutz, S., Prange, L.,
 452 Sośnica, K., Mervart, L., and Jäggi, A.: CODE's new solar radiation pressure model
 453 for GNSS orbit determination, *J. Geod.*, 89, 775-791, 2015.
- 454 7. Ballu, V., Gravelle, M., Wöppelmann, G., de Viron, O., Rebischung, P., Becker, M.,
 455 and Sakic, P.: Vertical land motion in the Southwest and Central Pacific from
 456 available GNSS solutions and implications for relative sea levels, *Geophys. J. Int.*,
 457 218(3), 1537-1551, doi:10.1093/gji/ggz247, 2019.
- 458 8. Blewitt, G., Kreemer, C., Hammond, W. C., and Gazeaux, J.: MIDAS robust trend
 459 estimator for accurate GPS station velocities without step detection, *J. Geophys. Res.:*
 460 *Solid Earth*, 121, 2054-2068, doi:10.1002/2015JB012552, 2016.
- 461 9. Blewitt, G., Hammond, W. C., and Kreemer, C.: Harnessing the GPS data explosion
 462 for interdisciplinary science, *Eos*, 99, 1–2, doi:10.1029/2018EO104623, 2018.
- 463 10. Böhm, J., Werl, B., and Schuh, H.: Troposphere mapping functions for GPS and very
 464 long baseline interferometry from European Centre for Medium-Range Weather
 465 Forecasts operational analysis data, *J. Geophys. Res.* 111, B02406, 2006.
- 466 11. Carter, W. E. (Ed.): Report of the survey workshop of the IAPSO tide gauge benchmark
 467 fixing committee, Report of a meeting held 13-15 December 1993 at the Inst. of
 468 Oceanog. Sci., Deacon Lab., NOAA Tech. Rep., NOSOES0006, 1994.
- 469 12. Chen, G., and Herring, T.A.: Effects of atmospheric azimuthal asymmetry on the
 470 analysis of space geodetic data, *J. Geophys. Res.* 102, 20489-20502, 1997.
- 471 13. Desai, S. D., and Sibois, A. E.: Evaluating predicted diurnal and semidiurnal tidal
 472 variations in polar motion with GPS-based observations, *J. Geophys. Res.: Solid Earth*,
 473 121(7), 5237-5256, doi:10.1002/2016JB013125, 2016.
- 474 14. Dill, R., and Döbbslaw, H. (2013). Numerical simulations of global-scale high-resolution
 475 hydrological crustal deformations, *J. Geophys. Res.: Solid Earth*, 118(9), 5008-5017,
 476 doi:10.1002/jgrb.50353, 2013.
- 477 15. Frederikse, T., Landerer, F., Caron, L., Adhikari, S., et al.: The causes of sea-level rise
 478 since 1900, *Nature*, 584, 393-397, doi: 10.1038/s41586-020-2591-3, 2020.
- 479 16. Gazeaux, J., Williams, S., King, M., Bos, M., Dach, R., Deo, M., Moore, A.W., Ostini,
 480 L., Petrie, E., Roggero, M., Teferle, F.N., Olivares, G., and Webb, F.H.: Detecting
 481 offsets in GPS time series: First results from the detection of offsets in GPS experiment,
 482 *J. Geophys. Res.: Solid Earth*, 118(5), 2397-2407, doi:10.1002/jgrb.50152, 2013.
- 483 17. Gobron, K., Rebischung, P., Van Camp, M., Demoulin, A., and de Viron, O.: Influence
 484 of aperiodic non-tidal atmospheric and oceanic loading deformations on the stochastic
 485 properties of global GNSS vertical land motion time series, *J. Geophys. Res.: Solid*
 486 *Earth*, 126, e2021JB022370, doi:10.1029/2021JB022370, 2021.



18. Gobron, K., Rebischung, P., de Viron, O., Demoulin, A., and Van Camp, M.: Impact of offsets on assessing the low-frequency stochastic properties of geodetic time series, *Journal of Geodesy*, 96, 42, <https://doi.org/10.1007/s00190-022-01634-9>.
19. Gravelle, M., Wöppelmann, G., M., Gobron, K., Altamimi, Z., Guichard, M., Herring, T., Rebischung, P.: The ULR-repro3 GPS data reanalysis solution (aka ULR7a), SONEC Data Center, https://doi.org/10.26166/sonel_uls7a, 2022.
20. Griffiths, J., and Ray, J.: Impacts of GNSS position offsets on global frame stability, *Geophys. J. Int.*, 204, 480–487, doi:10.1093/gji/ggv455, 2016.
21. Hamlington, B.D., Gardner, A.S., Ivins, E., *et al.*: Understanding of contemporary regional sea-level change and the implications for the future, *Rev. Geophys.*, 58, e2019RG0000672, 2020.
22. Hammond, W.C., Blewitt, G., Kreemer, C., and Nerem, R.S.: GPS imaging of global vertical land motion for studies of sea level rise, *J. Geophys. Res.: Solid Earth*, 126, e2021JB022355, doi:10.1029/2021JB022355, 2021.
23. Heflin, M.B., *et al.*: Global geodesy using GPS without fiducial sites, *Geophys. Res. Lett.*, 19, 131–134, 1992.
24. Herring, T.A., Floyd, M.A., and McClusky, S.C.: GLOBK Reference Manual, release 10.6, June 16th, 2015.
25. Herring, T.A., King, R.W., Floyd, M.A., King, R.W. and McClusky, S.C.: GAMIT Reference Manual, release 10.7, June 7th, 2018.
26. IOC: Global Sea-Level Observing System (GLOSS) Implementation Plan (2012), IOC Tech. Ser., Vol. 100, 41 pp., 2012.
27. Johnston, G., Riddell, A., and Hausler, G.: The International GNSS Service, Springer Handbook of Global Navigation Satellite Systems, 967–982, doi:10.1007/978-3-319-42928-1_33, 2017.
28. Koch, K.: Maximum likelihood estimate of variance components, *Bulletin Géodésique*, 60(4), 329–338, doi:10.1007/BF02522340, 1986.
29. Kouba, J.: A simplified yaw-attitude model for eclipsing GPS satellites, *GPS Solut.*, 13, 1–12, doi: 10.1007/s10291-008-0092-1, 2009.
30. Lagler, K., Schindelegger, M., Böhm, J., Krásná, H., Nilsson, T.: GPT2: Empirical slant delay model for radio space geodetic techniques, *Geophys. Res. Lett.* 40, 1069–1073, doi:10.1002/grl.50288, 2013.
31. Lyard, F.H., Allain, D.J., Cancet, M., Carrère, L., and Picot, N.: FES2014 global ocean tide atlas: Design and performance, *Ocean Sci.*, 17, 615–649, 2021.
32. Männel, B., Schöne, T., Bradke, M., and Schuh, H.: Vertical land motion at tide gauges observed by GNSS: a new GFZ-TIGA solution, IAG Symposia, 2022.
33. Magnan, A.K., Schipper, E.L.F., and Duvat, V.K.E.: Frontiers in climate change adaptation science: advancing guidelines to design adaptation pathways, *Curr. Clim. Change Rep.*, 6, 166–177, doi:10.1007/s40641-020-00166-8, 2020.
34. Marcos, M., Wöppelmann, G., Matthews, A., Ponte, R. M., Birol, F., Ardhuin, F., Coco, G., Santamaria-Gomez, A., Ballu, V., Testut, L., Chambers, D., and Stopa, J.E.: Coastal sea level and related fields from existing observing systems, *Surv. Geophys.*, 40, 1293–1317, doi:10.1007/s10712-019-09513-3, 2019.
35. Métivier, L., Collilieux, X., Lercier, D., Altamimi, Z., and Beauducel, F.: Global coseismic deformations, GNSS time series analysis, and earthquake scaling laws, *J. Geophys. Res.: Solid Earth*, 119, 9095–9109, 2014.
36. Patterson, H.D., and Thompson, R.: Recovery of inter-block information when block sizes are unequal, *Biometrika*, 58(3), 545–554, doi: 10.1093/biomet/58.3.545, 1971.



- 535 37. Pavlis, N.K., Holmes, S.A., Kenyon, S.C., and Factor, J.K.: The development and
 536 evaluation of the Earth Gravitational Model 2008 (EGM2008), *J. Geophys. Res.*,
 537 117(B4), B04406, doi: 10.1029/2011JB008916, 2012.
- 538 38. Penna, N. T., and M. P. Stewart: Aliased tidal signatures in continuous GPS height time
 539 series, *Geophys. Res. Lett.*, 30(23), 2184, doi:10.1029/2003GL018828, 2003.
- 540 39. Petit, G., and Luzum, B.: IERS conventions, Tech. Note 36, Bureau International des
 541 Poids et Mesures, Sevres (France), 2010. Online : <https://iers-conventions.obspm.fr/>
- 542 40. Poitevin, C., Wöppelmann, G., Raucoules, D., Le Cozannet, G., Marcos, M., and Testut,
 543 L.: Vertical land motion and relative sea level changes along the coastline of Brest
 544 (France) from combined space-borne geodetic methods, *Remote Sens. Environ.*, 222,
 545 275-285, doi:10.1016/j.rse.2018.12.035, 2019.
- 546 41. Ray, J., Altamimi, Z., Collilieux, X., and van Dam, T.: Anomalous harmonics in the
 547 spectra of GPS position estimates, *GPS Solut.*, 12(1), 55-64, doi: 10.1007/s10291-007-
 548 0067-7, 2008.
- 549 42. Rebischung, P.: Terrestrial frame solutions from the third IGS reprocessing, EGU
 550 General Assembly, 19-30 April 2021, EGU21-2144, [https://doi.org/10.5194/egusphere-](https://doi.org/10.5194/egusphere-egu21-2144)
 551 [egu21-2144](https://doi.org/10.5194/egusphere-egu21-2144), 2021.
- 552 43. Rebischung, P., Altamimi, Z., Ray, J., and Garayt, B.: The IGS contribution to
 553 ITRF2014, *J. Geodesy*, 90, 611-630, doi: 10.1007/s00190-016-0897-6, 2016.
- 554 44. Rebischung, P., Collilieux, X., Métivier, L., Altamimi, Z., and Chanard, K.: Analysis of
 555 IGS repro3 Station Position Time Series, AGU Fall Meeting, 13-17 Dec. 2021, doi:
 556 10.1002/essoar.10509008.1, 2021.
- 557 45. Sanli, D. U., and Blewitt, G.: Geocentric sea level trend using GPS and >100-year tide
 558 gauge record on a postglacial rebound nodal line, *J. Geophys. Res.*, 106(B1), 713-719,
 559 doi:10.1029/2000JB900348, 2001.
- 560 46. Santamaria-Gomez, A., and Ray, J.: Chameleonic noise in GPS position time series, *J.*
 561 *Geophys. Res.: Solid Earth*, 126, e2020JB019541, doi: 10.1029/2020JB019541, 2021.
- 562 47. Santamaria-Gomez, A., Bouin, M.-N., Collilieux, X., and Wöppelmann, G.: Correlated
 563 errors in GPS position time series: Implications for velocity estimates, *J. Geophys. Res.*,
 564 116, B01405, doi:10.1029/2010JB007701, 2011.
- 565 48. Santamaria-Gomez, A., Gravelle, M., Dangendorf, S., Marcos, M., Spada, G., and
 566 Wöppelmann, G.: Uncertainty of the 20th century sea-level rise due to vertical land
 567 motion errors, *Earth and Planetary Science Letters*, 473, 24-32, 2017.
- 568 49. Schöne, T., Schön, N., and Thaller, D.: IGS Tide gauge benchmark monitoring pilot
 569 project (TIGA): scientific benefits, *J. Geodesy*, 83, 249-261, doi: 10.1007/s00190-008-
 570 0269-y, 2009.
- 571 50. Springer, T.A., Beutler, G., and Rothacher, M.: A new solar radiation pressure model
 572 for GPS, *Adv. Space Res.*, 23 (4), 673-676, doi:10.1016/S0273-1177(99)00158-1,
 573 1999.
- 574 51. Steigenberger, P., Rothacher, M., Dietrich, R., Fritsche, M., Rülke, A., and Vey, S.:
 575 Reprocessing of a global GPS network, *J. Geophys. Res.*, 111, B05402,
 576 doi:10.1029/2005JB003747, 2006.
- 577 52. Williams, S.D.P., Bock, Y., Fang, P., Jamason, P., Nikolaidis, R.M., Prawirodirdjo, L.,
 578 Miller, M., and Johnson, D.J.: Error analysis of continuousGPS position time series, *J.*
 579 *Geophys. Res.*, 109, B03412, doi:10.1029/2003JB002741, 2004.
- 580 53. Wöppelmann, G., and Marcos, M.: Vertical land motion as a key to understanding sea
 581 level change and variability, *Rev. Geophys.*, 54, 64-92, 2016.
- 582 54. Wöppelmann, G., Martin Miguez, B., Bouin, M.-N., and Altamimi: Geocentric sea-
 583 level trend estimates from GPS analyses at relevant tide gauges world-wide, *Glob.*
 584 *Planet. Change*, 57, 396-406, doi:10.1016/j.gloplacha.2007.02.002, 2007.



- 585 55. Wöppelmann, G., Letetrel, C., Santamaria, A., Bouin, M.-N., Collilieux, X., Altamimi,
586 Z., Williams, S. D. P., and Martin Miguez, B.: Rate of sea-level change over the past
587 century in a geocentric reference frame, *Geophys. Res. Lett.*, 36, L12607, doi:
588 10.1029/2009GL038720, 2009.
- 589 56. Wöppelmann, G., Gravelle, M., and Testut, L.: SONEL sea-level observing
590 infrastructure: French contribution to the IUGG Centennial in 2019 and beyond,
591 *Collection du Bureau des Longitudes*, 1, 43-53, ISBN: 978-2-491688-08-0, 2021.
- 592 57. Woodworth, P. L., Melet, A., Marcos, M., Ray, R.D., Wöppelmann, G., Sasaki, Y. N.,
593 Cirano, M., Hibbert, A., Huthnance, J. M., Monserrat, S., and Merrifield, M. A.: Forcing
594 factors affecting sea level changes at the coast, *Surv. Geophys.*, 40, 1351-1397, 2021.
- 595 58. Wu, J.T., Wu, S.C., Hajj, G.A., Bertiger, W.I., and Lichten, S.M.: Effects of antenna
596 orientation on GPS carrier phase, *Manuscr. Geodaet.* 18, 91-98, 1993.
597